

Gain Scheduled Control of a Solar Power Plant

Tor A. Johansen^{1*}, Kenneth J. Hunt² and Idar Petersen¹

¹ Norwegian University of Science and Technology,
Department of Engineering Cybernetics, N-7491 Trondheim, Norway.

² Centre for Systems and Control, Department of Mechanical Engineering,
University of Glasgow, Glasgow G12 8QQ, Scotland.

February 15, 2000

Abstract

The application of gain-scheduled control to a pilot-scale solar power plant is described. A field of parabolic collectors focus the solar radiation onto a tube where oil is pumped through in order to collect the solar power. The control problem is to keep the temperature of the oil leaving the field at its desired value by manipulating the oil pump flow rate. It is shown that gain-scheduling can effectively handle the plant nonlinearities, using high-order local linear ARX models that form the basis for the design of local linear controllers using pole placement.

Keywords. Solar power plant, nonlinear control, gain scheduling, system identification.

1 Introduction

The application of gain scheduled control to a pilot-scale solar power plant, Plataforma Solar de Almeria (PSA), is described. A field of parabolic collectors focus the solar radiation onto a tube where oil is pumped through in order to collect the solar power. An important control problem is to keep the temperature of the oil flow leaving the field at its setpoint, despite variations in solar radiation and oil inlet temperature, in order to avoid disturbances downstream to the power conversion system and to avoid damage due to overheating of the oil. The main manipulated variable is the oil flow rate.

*Email: Tor.Arne.Johansen@itk.ntnu.no

This problem has been studied experimentally at PSA by numerous research groups investigating different control strategies and design methods, see e.g. (Camacho *et al.* 1997, Silva *et al.* 1997). It is recognized that the plant dynamics contain significant nonlinear effects due to variations in the oil flow rate. A traditional gain-scheduling approach is taken, using multiple local linear controllers, each designed by pole-placement (Åström and Wittenmark 1997, Hunt and Johansen 1997) based on local linear ARX models which are identified using the methods and software described in (Hunt and Johansen 1997, Johansen *et al.* 1998). Other variations of gain-scheduling have been applied to this problem. In (Camacho *et al.* 1994, Camacho *et al.* 1997) the local linear design was based on generalized predictive control and local linear ARX models, with excellent results. An adaptive gain-scheduled LQ design approach, also based on local linear ARX models, was investigated by Pickhardt (1998). A control strategy based on switching between multiple local linear models/controllers was suggested and tested by Rato *et al.* (1997).

This paper is organized as follows: In section 2, a brief overview of the plant is given. A simple gain-scheduled control structure is derived in section 3, based on elementary energy balance considerations. A set of local linear models is described in section 4, and local linear controllers are designed and analysed in section 5. Experimental results are reported and discussed in section 6, and the paper ends with some conclusions in section 7.

2 Plant description

The ACUREX-field of Plataforma Solar de Almeria (PSA) is located in the southern part of Spain. Figures 1-2 shows photographs of the Acurex plant. The field is composed of 480 distributed solar collectors, arranged in 10 parallel loops. A simplified functional diagram of the Acurex plant is shown in Figure 3, (Camacho *et al.* 1997).

A collector uses the parabolic surface to focus the solar radiation onto a receiver tube, which is placed in the focal line of the parabola, cf. Figure 2. The heat-absorbing oil is pumped through the receiver tube, causing the oil to collect heat which is transferred through the receiver tube walls. The thermal energy developed by the field is pumped to the top of the thermal storage tank, whereupon the oil from the top of the storage tank can be fed to a power generating system, a desalination plant or to an oil-cooling system, if needed. The oil outlet from the storage tank to the field is at the bottom of the storage tank. For the initial startup of the plant, the system is provided with a three way valve which allows the oil to be circulated in the field until the outlet temperature is adequate to enter the storage tank. The oil pump which pumps the oil from the storage tank, through the collector tubes and into the top of the storage tank is located at the field inlet. To ensure that the collectors give optimum solar absorption, every collector row has a sun



Figure 1: Acurex, the distributed collector field at PSA, Almeria, Spain.



Figure 2: Parabolic collector.

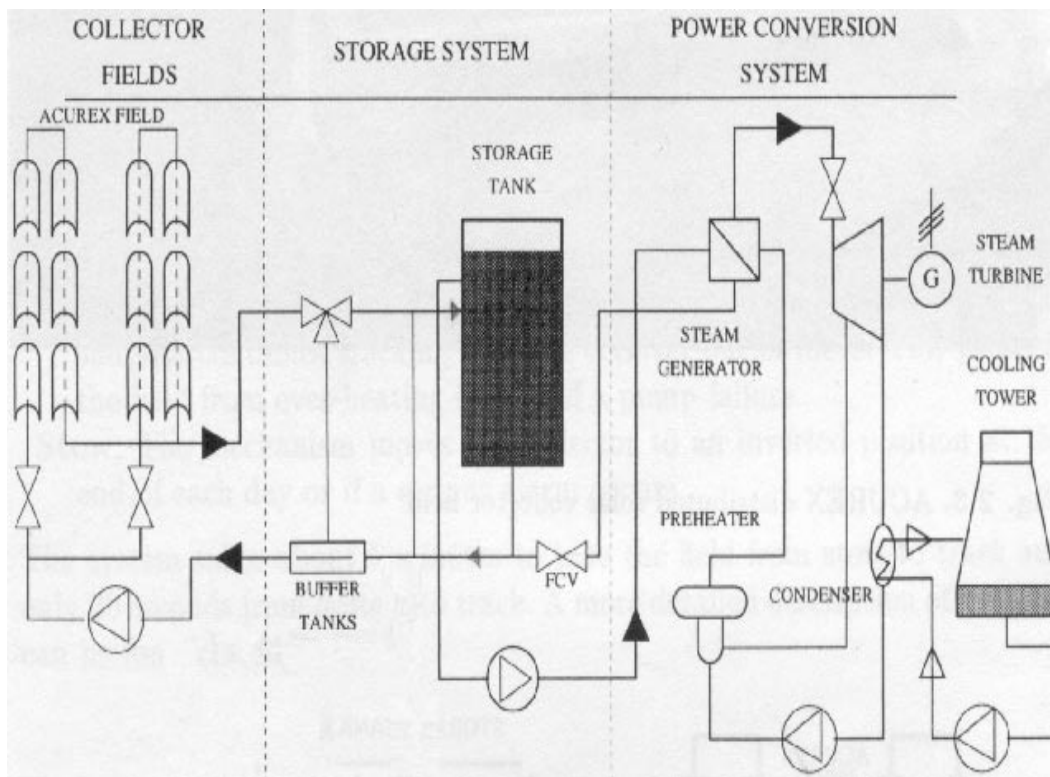


Figure 3: Functional diagram of the plant.

tracking system fitted to it.

The data acquisition system for the plant provides the following data: the solar intensity, inlet temperature to the field, outlet temperature of each loop and two other outlet temperatures between the field and storage tank, the current oil pump flow and requested value, and the tracking status of the collectors.

The plant can generate 1.2 MW of peak power with beam solar radiation of 900 W/m^2 . The oil-storage tank has a capacity of 140 m^3 , which allows for storage of 2.3 thermal MWh for an inlet temperature of 210°C and an outlet temperature of 290°C .

The operation limits for the oil pump are between 2.0 - 10.0 litres per second. The minimum value is there for safety and mainly to reduce the risk of the oil being decomposed, which happens when the oil temperature exceeds 305°C . The consequence of exceeding the maximum oil temperature is that all the oil may have to be changed. Another important restricting element in this system is the difference between the field's inlet and outlet oil temperatures. A suitable or normal difference is around or less than 70°C . If the difference is higher than 100°C , then there is a significant risk of causing oil leakage due to high oil pressure in the pipe system.

A control system for this plant has the objective of maintaining the outlet temperature (in this case the average outlet temperature of all the parallel loops) at a desired level in spite of disturbances like

solar irradiation (clouds and atmospheric phenomena), mirror reflectivity and inlet oil temperature. The oil flow rate is manipulated by the control system through commands to the pump. It should be noticed that the primary energy source, solar radiation, cannot be manipulated. The performance measures of the control system are to keep the oil outlet temperature close to its setpoint, and to avoid oscillations in the oil pump flow rate.

3 Control structure

Based on the concentrated parameter model of Camacho *et al.* (1997) the rate of change of the total internal energy of the field can be described by:

$$C \frac{dT_{out}}{dt} = n_o S I - q p_{cp} (T_{out} - T_{in}) \quad (1)$$

where T_{out} is the oil temperature at the field outlet (computed as the average temperature at the outlets of the 10 loops), T_{in} is the oil temperature at the field inlet, I is corrected effective solar radiation, q is the volumetric oil flow rate, n_o is the collector optical efficiency, S is the field effective surface, C is the specific thermal capacity of the oil, and p_{cp} accounts for the product and quotient of characteristic magnitudes (areas, thermal capacities, etc).

For convenience, define $m = n_o S$, we introduce $\Delta T = T_{out} - T_{in}$, and assume T_{in} to be slowly time-varying, which gives $\frac{d}{dt} \Delta T \approx \frac{d}{dt} T_{out}$. The energy balance can now be rewritten:

$$C \frac{d}{dt} \Delta T = m I - q p_{cp} \Delta T \quad (2)$$

From the control point of view, ΔT is the controlled variable, q is the manipulated variable, and I is a disturbance. The other symbols can be viewed as constant parameters.

At steady state, it is observed that

$$\Delta T = \frac{m I}{q p_{cp}} \quad (3)$$

In other words, the steady state oil temperature change over the field is proportional to the solar radiation (the power input) and inversely proportional to the oil flow rate (or equivalently, proportional to the residence time of the oil in the field). A linearization of (2) about an operating point $(I^0, q^0, \Delta T^0)$ leads to the model

$$C \frac{d}{dt} \Delta T = m I - q^0 p_{cp} \Delta T - q p_{cp} \Delta T^0 + q^0 p_{cp} \Delta T^0 \quad (4)$$

which can be rewritten as

$$\frac{C}{q^0 p_{cp}} \frac{d}{dt} \Delta T + \Delta T = \frac{m}{q^0 p_{cp}} I - \frac{\Delta T^0}{q^0} (q - q^0) \quad (5)$$

Hence, the time-constant and gain of the linearized model depend on the oil flow rate and temperature increase over the field. An ideal gain-scheduled controller should therefore contain a feedback that is scheduled on ΔT and q in order to capture the nonlinearities. Furthermore, it might also contain a feedforward from I :

$$q_{ff} = \frac{mI}{p_{cp}\Delta T^*} \quad (6)$$

where ΔT^* is the desired temperature change. We want to restrict the complexity of the gain-scheduled controller and avoid scheduling on ΔT since it is, in general, advantageous to schedule on auxiliary variables such as I rather than the output ΔT (Rugh 1991). Furthermore, we require that the point of linearization $(I^0, q^0, \Delta T^0)$ is an equilibrium point. It can be argued that the flow-rate is the main variable leading to nonlinearities in this plant (Camacho *et al.* 1997), so we eliminate ΔT^0 from (5) using (3):

$$\frac{C}{q^0 p_{cp}} \frac{d}{dt} \Delta T + \Delta T = \frac{mI}{q^0 p_{cp}} - \frac{mI^0}{(q^0)^2 p_{cp}} (q - q^0) \quad (7)$$

This leads to a gain-scheduled controller where the feedback is scheduled on the flow-rate q and solar radiation I . The reason for this can be seen from (7) where it is evident that the gain of the linearized model is proportional to $I^0/(q^0)^2$ and the time constant of the linearized model is proportional to $1/q^0$. The controller might also in this case include a feedforward from I in order to improve disturbance rejection. An overview of the controller is provided in Figure 4, and the decomposition of the operating range $0 \leq I \leq 1000 \text{ W/m}^2$ and $2 \text{ l/s} \leq q \leq 10 \text{ l/s}$ is illustrated in Figure 5. This decomposition is selected such that the gain and time constant of the linearization of the simple model (7) varies with less than a factor of 2 between any neighbouring regimes. Thus, assuming the local models are exactly correct at the center points of their corresponding regimes, the interpolated model gain and time constant are never more than a factor of $\sqrt{2}$ wrong. The weighting functions used in the interpolation are shown in Figure 6. They are designed to give a smooth transition between the operating regimes.

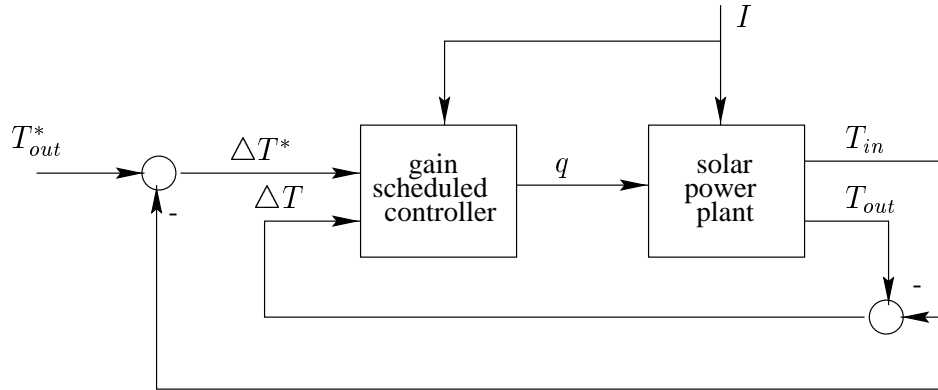


Figure 4: Structure of the gain-scheduled controller.

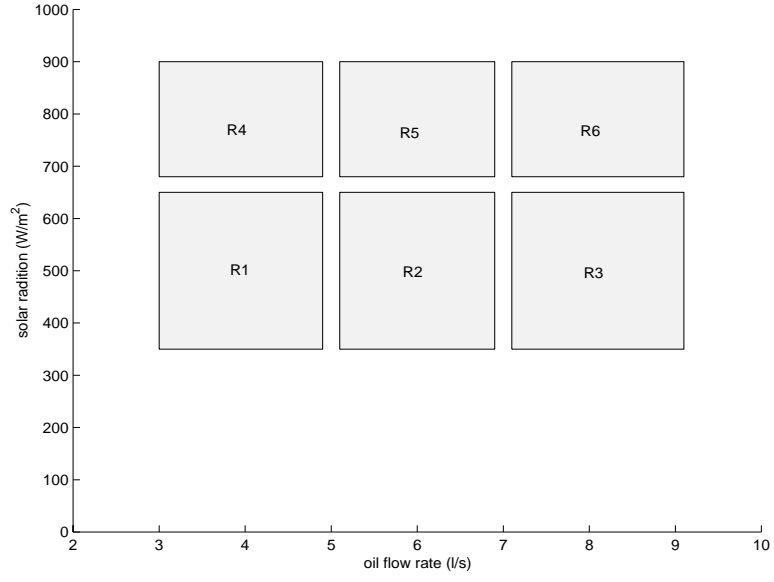


Figure 5: Operating regimes of the gain-scheduled controller.

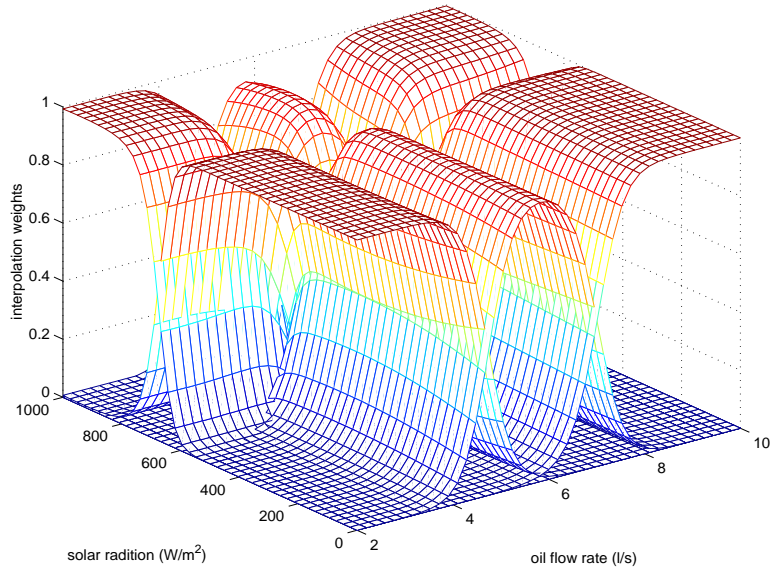


Figure 6: Weighting functions used in the gain-scheduler.

4 Local linear models

The concentrated model (2) and its linearization (5) are very simple models that characterize the main dynamics of the plant. However, they are not sufficiently accurate to develop local linear controllers or a nonlinear gain scheduled controller with high performance. The reason for this is that the concentrated parameter model fails to capture some important dynamic phenomena of the plant, namely anti-resonant modes (Meaburn and Hughes 1993). These modes are present at frequencies around the desired/achievable bandwidth of the closed loop and must therefore be accurately modelled in order to achieve the highest possible bandwidth together with adequate robustness.

The presence of anti-resonant modes can be explained as follows: consider a sinusoidal perturbation of the flow rate about some nominal flow rate with a period equal to the residence-time of the oil in the collector loop. A slight increase of the flow rate will lead to reduced temperature change due to reduction of the residence-time, and vice versa. However, because the period of the perturbation equals the residence-time and the solar heat flux is constant over the field, the positive and negative temperature perturbations due to the flow rate perturbations over the period cancels each other exactly. Hence, the magnitude of the transfer function from oil flow rate q to temperature change ΔT is zero (theoretically) at the frequencies corresponding to the residence-time and its harmonic frequencies. In practice, the transfer function magnitude does not reduce completely to zero at the anti-resonance frequencies, due to heat conduction and mixing. The transfer function from radiation I to temperature change ΔT can be seen to contain the same anti-resonant modes by considering a sinusoidal perturbation of the solar radiation in a similar manner.

The anti-resonance modes can be accurately described by a nonlinear distributed parameter model or by linear transfer-functions of sufficiently high order (Camacho *et al.* 1997). We have chosen to use local linear ARX models which are convenient for local linear controller design.

In accordance with the block diagram in Figure 4, we define the following variables:

$$\text{Output: } y(t) = \Delta T(t) = T_{out}(t) - T_{in}(t) \quad (8)$$

$$\text{Reference: } r(t) = \Delta T^*(t) = T_{out}^*(t) - T_{in}(t) \quad (9)$$

$$\text{Input: } u(t) = q(t) \quad (10)$$

$$\text{Disturbance: } v(t) = I(t) \quad (11)$$

Three local linear models were identified from experimental data, using locally weighted regression as described in (Johansen *et al.* 1998), corresponding to operating points with oil flow rates at 4 l/s, 6 l/s and 8 l/s, respectively. The plant was perturbed with PRBS signals of amplitude 0.5 l/s around all these operating points, see Figure 7 for an example with the PRBS data in the 6 l/s

regime. There were no major disturbances on the solar radiation during these tests. It is evident from (7) that the linearized plant gain is proportional to the solar radiation. Hence, the gain of the local linear models are corrected using the average solar radiation during each PRBS test such that they all correspond to a nominal solar radiation of 800 W/m². Furthermore, 3 new local models corresponding to a solar radiation of 500 W/m² were generated by reducing the gain accordingly. This gives a total of 6 local models for the 6 operating regimes, cf. Figure 5. Notice that the plant normally does not operate in steady state at solar raditions below 400 W/m².

Bode plots of the three local models corresponding to a solar radiation of 800 W/m² are shown in Figure 8, their parameters are given in Table 1, and their pole/zero locations are shown in Figure 9. The 3 local models at 500 W/m² only differ by a constant gain factor of 5/8. The sampling interval in the models and controllers is 30 s. The selection of model order is made after careful validation and is consistent with the models presented in e.g. (Camacho *et al.* 1997).

R1	$\frac{y(t)}{u(t)} = \frac{-0.07887q^{-1}-0.4417q^{-2}+0.3062q^{-3}+0.1664q^{-4}-0.1343q^{-5}-0.0260q^{-6}-0.04364q^{-7}}{1-2.177q^{-1}+1.569q^{-2}-0.373q^{-3}}$
R2	$\frac{y(t)}{u(t)} = \frac{-0.2268q^{-1}-0.2736q^{-2}+0.2714q^{-3}-0.03576q^{-4}-0.09612q^{-5}-0.01281q^{-6}-0.1112q^{-7}}{1-2.092q^{-1}+1.519q^{-2}-0.3819q^{-3}}$
R3	$\frac{y(t)}{u(t)} = \frac{-0.1611q^{-1}-0.2916q^{-2}+0.1157q^{-3}-0.05857q^{-4}-0.1031q^{-5}-0.06979q^{-6}-0.07169q^{-7}}{1-1.744q^{-1}+1.065q^{-2}-0.2091q^{-3}}$

Table 1: Local models.

Notice in particular the following observations:

- The phase starting at +180° is due to the negative gain of the transfer functions.
- The first and second anti-resonance modes are easy to observe and their frequencies depend on the flow-rate (or residence time) as expected.
- The phase at the first anti-resonance frequency is about -180° (when taking into account the negative gain which corresponds to -180°). In order to attain high bandwidth it is therefore important to have an accurate model of the anti-resonance modes. We have experienced that lower-order models are not sufficiently accurate and lead to oscillations. This is confirmed by other researchers' experiences, e.g. (Meaburn and Hughes 1993, Camacho *et al.* 1997).
- The anti-resonance modes of the local model in the 4 l/s region do not appear as pronounced as the others. We believe that this is model inaccuracy, possibly caused by a combination of too short an experiment and too high a PRBS signal amplitude leading to some smoothing of the model's frequency response because the anti-resonance frequency depends on the signal amplitude.
- The changing plant characteristics can also be seen from the pole-zero plots. The anti-resonance modes can be clearly identified from the complex-conjugate plant zeros. It can also be seen from the positions of the dominating open-loop poles that the open-loop system

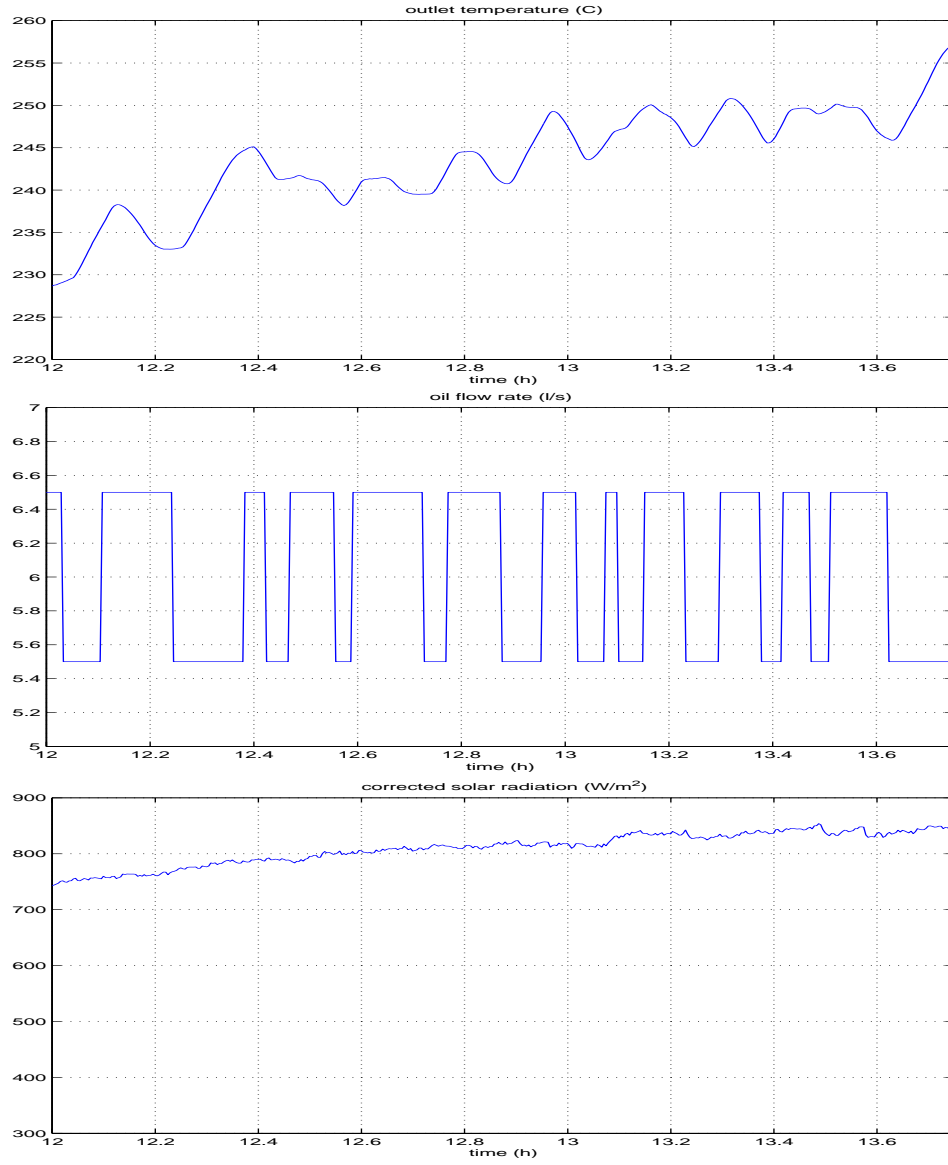


Figure 7: Identification data for the 6 l/s local models: Average loop outlet temperature, commanded oil flow rate and solar radiation.

becomes faster (the poles move away from the unit circle) as the flowrate increases.

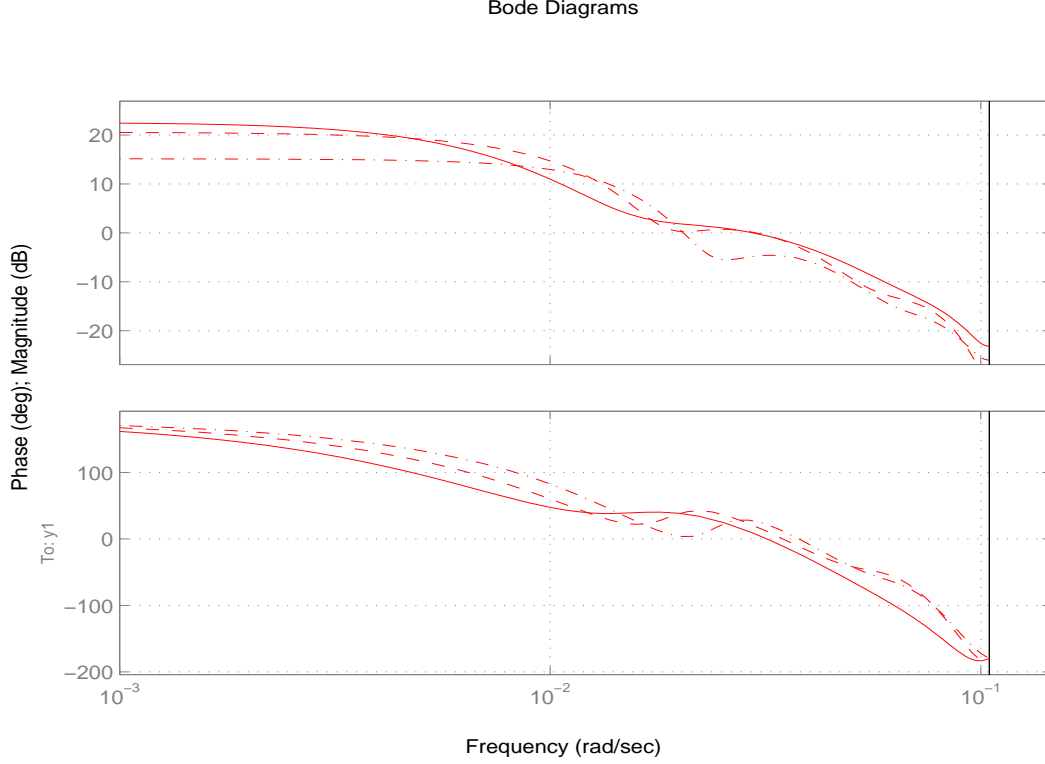


Figure 8: Bode plots for local models in regimes R1 (4 l/s, solid), R2 (6 l/s, dashed) and R3 (8 l/s, dashed-dotted).

5 Local linear controllers

The local ARX models were used to design local linear RST controllers. Each local controller has the form

$$u(t) = \frac{1}{R(q^{-1})(1 - q^{-1})}(T(q^{-1})r(t) - S(q^{-1})y(t)). \quad (12)$$

The term $1 - q^{-1}$ provides integral action in the controller. Each local controller is designed using pole assignment by solving the linear equation

$$A(q^{-1})R(q^{-1})(1 - q^{-1}) + B(q^{-1})S(q^{-1}) = A_m(q^{-1})A_o(q^{-1}) \quad (13)$$

for R and S . The design problem thus becomes that of choosing the closed-loop pole polynomial A_m and the observer polynomial A_o . The poles of each of these terms is chosen via a time-domain approach where the desired damping and risetime of a standard second-order transfer function are selected, and the polynomial A_m (or A_o) is computed as the denominator of the resulting discrete-time transfer function. Finally, the polynomial T is chosen to include A_o as a factor, and is scaled

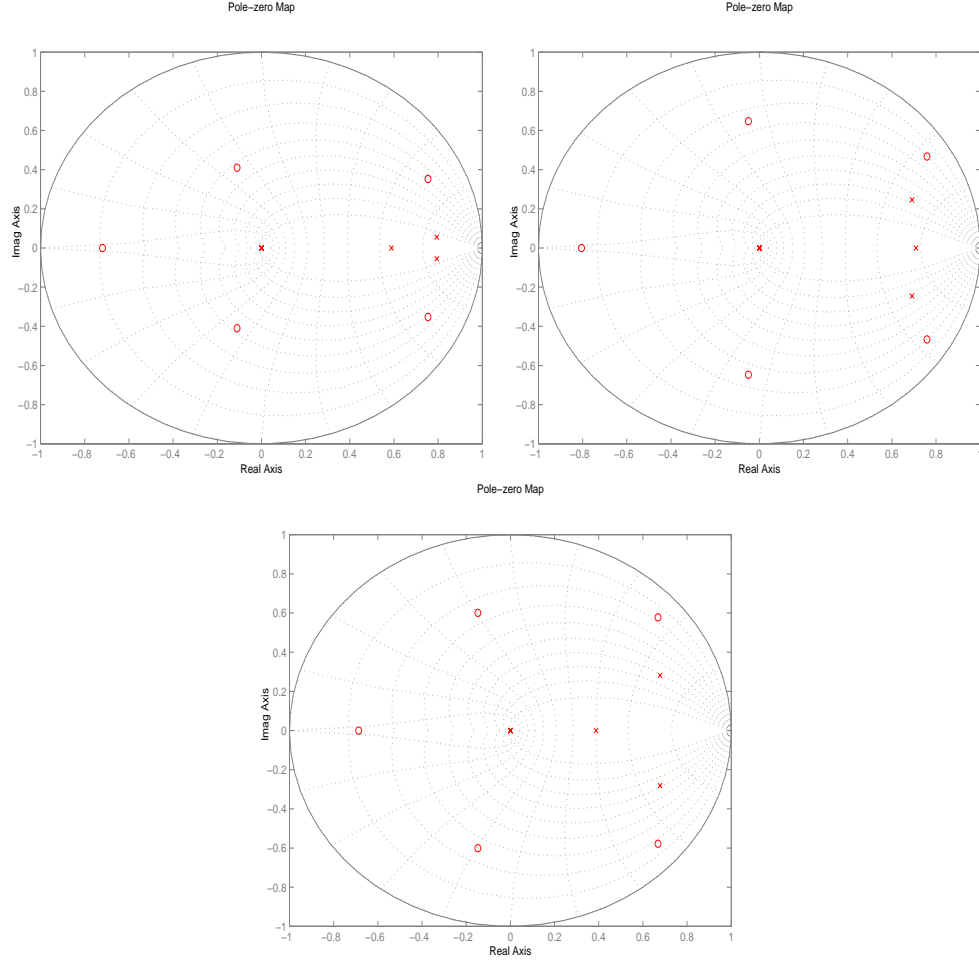


Figure 9: Pole/zero plots for local models in regimes R1 (4 l/s), R2 (6 l/s) and R3 (8 l/s).

to give unity steady-state gain in the closed-loop transfer function from r to y . Further details on the design approach can be found in (Hunt and Johansen 1997, Åström and Wittenmark 1997).

In general, we require low frequency roll-off of the sensitivity function, which is achieved by integral action. We also require high-frequency roll-off of the complementary sensitivity function, which is achieved by adding a 2nd order observer polynomial. These requirements ensure robustness against low- and high-frequency perturbations, respectively. In the crossover region the design is chosen with sufficient gain and phase margins, as well as small peaking of the sensitivity and complementary sensitivity functions. The control design parameters used for the three flowrate regimes are listed in Table 2, leading to closed loop poles that can be seen in Figure 10. Compared to the open loop poles in Figure 9, the closed loop poles have moved towards the origin in order to get high bandwidth. Furthermore, no attempt was made to damp the resonant open loop poles in the closed loop design because such a design might not be expected to be very robust. Figures 11 - 14 show the open loop transfer functions, input disturbance to output transfer functions, reference to output transfer functions (complementary sensitivity function), and output disturbance to output transfer functions (sensitivity function), respectively. It can be seen that the requirements of low- and high-frequency roll-off are met. From these plots we can also observe that in the crossover region the gain margin is larger than 8 dB in all regimes and the phase margin is larger than 60° in all regimes.

	4 l/s region	6 l/s region	8 l/s region
Rise-time	250 s and 180 s	180 s and 120 s	180 s and 120 s
Damping	0.99 and 0.7	0.99 and 0.7	0.99 and 0.7
Observer rise-time	90 s and 90 s	90 s and 90 s	90 s and 90 s
Observer damping	0.99 and 0.99	0.99 and 0.99	0.99 and 0.99

Table 2: Specification of the closed loop modes of the design.

6 Experimental results and discussion

6.1 Linear control

Figure 15 shows an experimental result with a linear controller. This linear controller was designed using the model from the 8 l/s operating regime, with the control design parameters listed in Table 2.

The top part of the plot shows the temperature setpoint and the measured temperature. The middle graph shows the control signal (i.e. the demanded flowrate), and the lower graph shows the

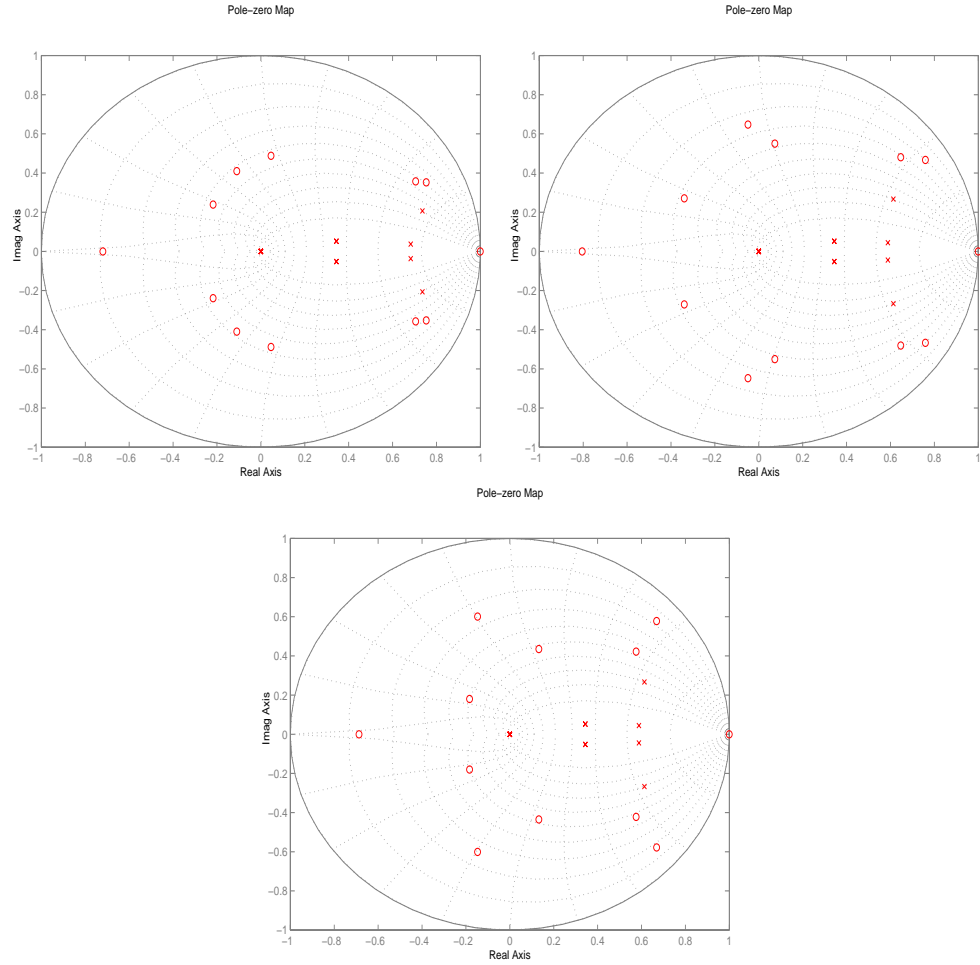


Figure 10: Pole/zero plots for the closed loop transfer function between disturbance $v(t)$ and output $y(t)$ in regimes R1 (4 l/s), R2 (6 l/s) and R3 (8 l/s).

Bode Diagrams

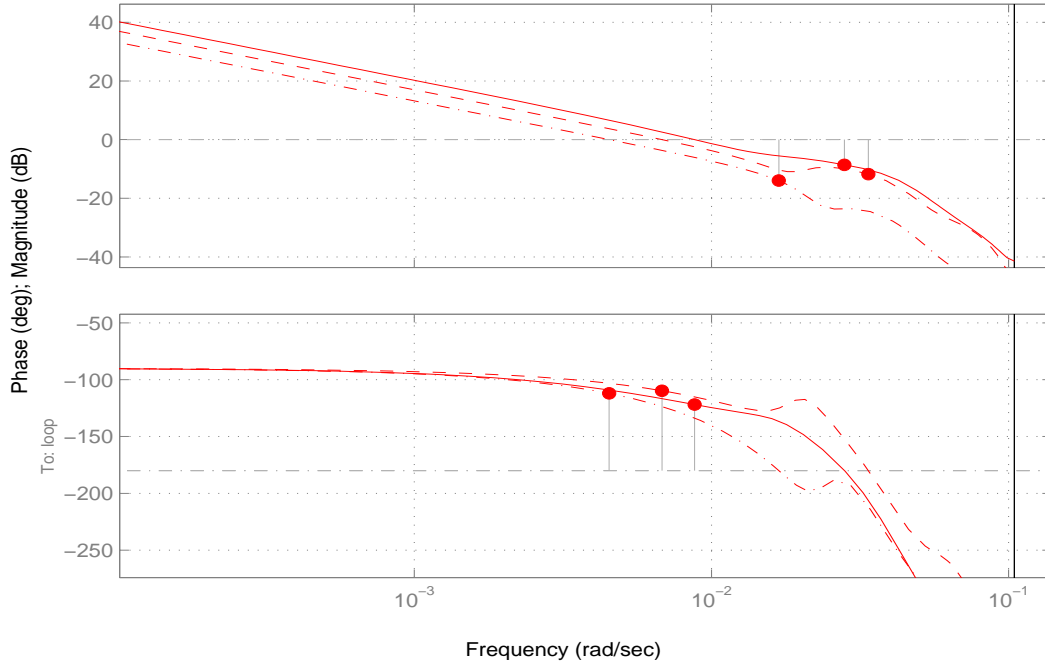


Figure 11: Bode plots of the open loop transfer functions in regimes R1 (4 l/s, solid), R2 (6 l/s, dashed) and R3 (8 l/s, dashed-dotted).

Bode Diagrams

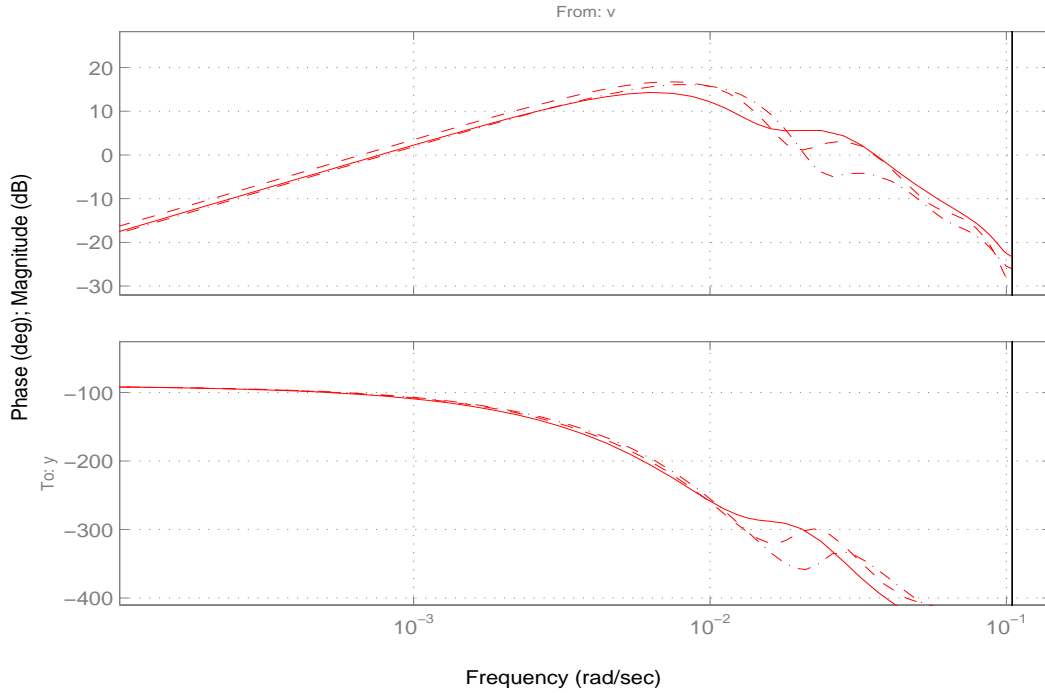


Figure 12: Bode plots of the transfer functions between input disturbances and output in regimes R1 (4 l/s, solid), R2 (6 l/s, dashed) and R3 (8 l/s, dashed-dotted).

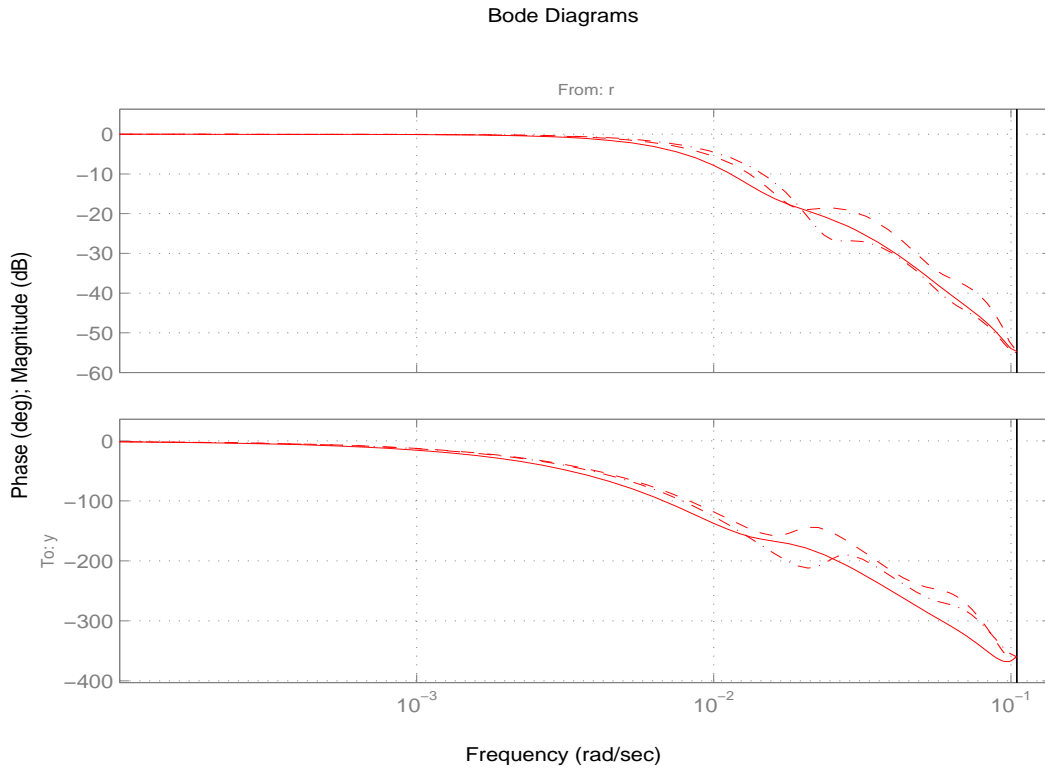


Figure 13: Bode plots of the transfer functions between reference and output (complementary sensitivity function) in regimes R1 (4 l/s, solid), R2 (6 l/s, dashed) and R3 (8 l/s, dashed-dotted).

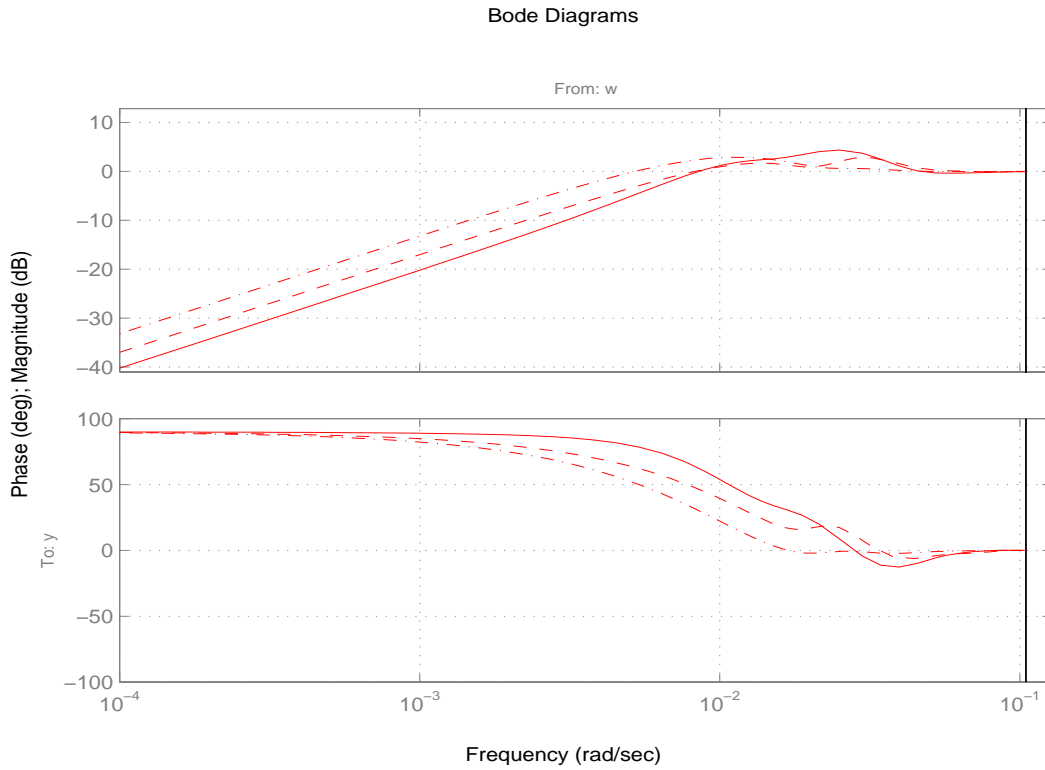


Figure 14: Bode plots of the transfer functions between output disturbances and output (sensitivity function) in regimes R1 (4 l/s, solid), R2 (6 l/s, dashed) and R3 (8 l/s, dashed-dotted).

measured solar radiation. The solar radiation shows only a slow variation during this experiment as the sun moves across the sky. No major disturbances (e.g. clouds) occurred.

This experiment illustrates that the linear controller works well only in the flow region near the operating point where the linear model was identified (around 8 l/s). This can be seen in the time from 13h to 13.6h. When the system operates with a lower flowrate around 6 l/s (near $t = 12.9$ h and beyond $t = 13.6$ h) the control performance is poor, with large overshoots, and a slightly oscillatory control signal.

6.2 Gain scheduled control

An experimental result with the gain scheduled controller is shown in figure 16. Again, during this experiment, the solar radiation did not suffer any sudden variations.

The result shows that the gain scheduled controller works very well across the flow range above 5 l/s, encompassing the chosen operating points of 6 l/s and 8 l/s. However, performance at the lower flowrate of 4 l/s is not as good, with significant overshoot and some oscillation of the control signal. The possible model inaccuracy of the gain-scheduled controller in the 4 l/s region was discussed above, and in particular, we believe that the local model for the 4 l/s operating point did not capture the anti-resonance mode accurately here, cf. Figure 8. This is reflected in the poor control performance in this region. We believe this situation can be improved by improving the model in this regime with an improved PRBS test signal. Furthermore, the nonlinearities are more pronounced at low flow rate (they are roughly proportional to $1/q$ as established by the simplified model analysis). Thus, a finer decomposition into operating regimes may be desirable as q becomes smaller. Furthermore, it can be seen from the Bode plots, Figures 11 - 14, that the design for the 4 l/s might be improved by reducing the bandwidth and thus also reducing the peaks of the sensitivity functions for this region, since the 4 l/s regime has the largest peak near the anti-resonance mode and also the smallest stability margins.

A complete comparison of the gain-scheduled controller presented here to the results from the literature is difficult because of variations in operational conditions and limited access time to the plant for fine tuning of the controllers. However, some observations can be made.

In the regions where the gain-scheduled pole placement controller is based on adequate models (in the 6 l/s and 8 l/s regions) the setpoint tracking performance is excellent, comparable to the results of the gain-scheduled generalized predictive controller reported in (Camacho *et al.* 1994). In both cases, the local linear controllers were scheduled on the oil flow rate.

When compared to the related approaches (Pickhardt 1998, Rato *et al.* 1997), the setpoint tracking performance of the gain-scheduled pole placement controller appears to be significantly better. One

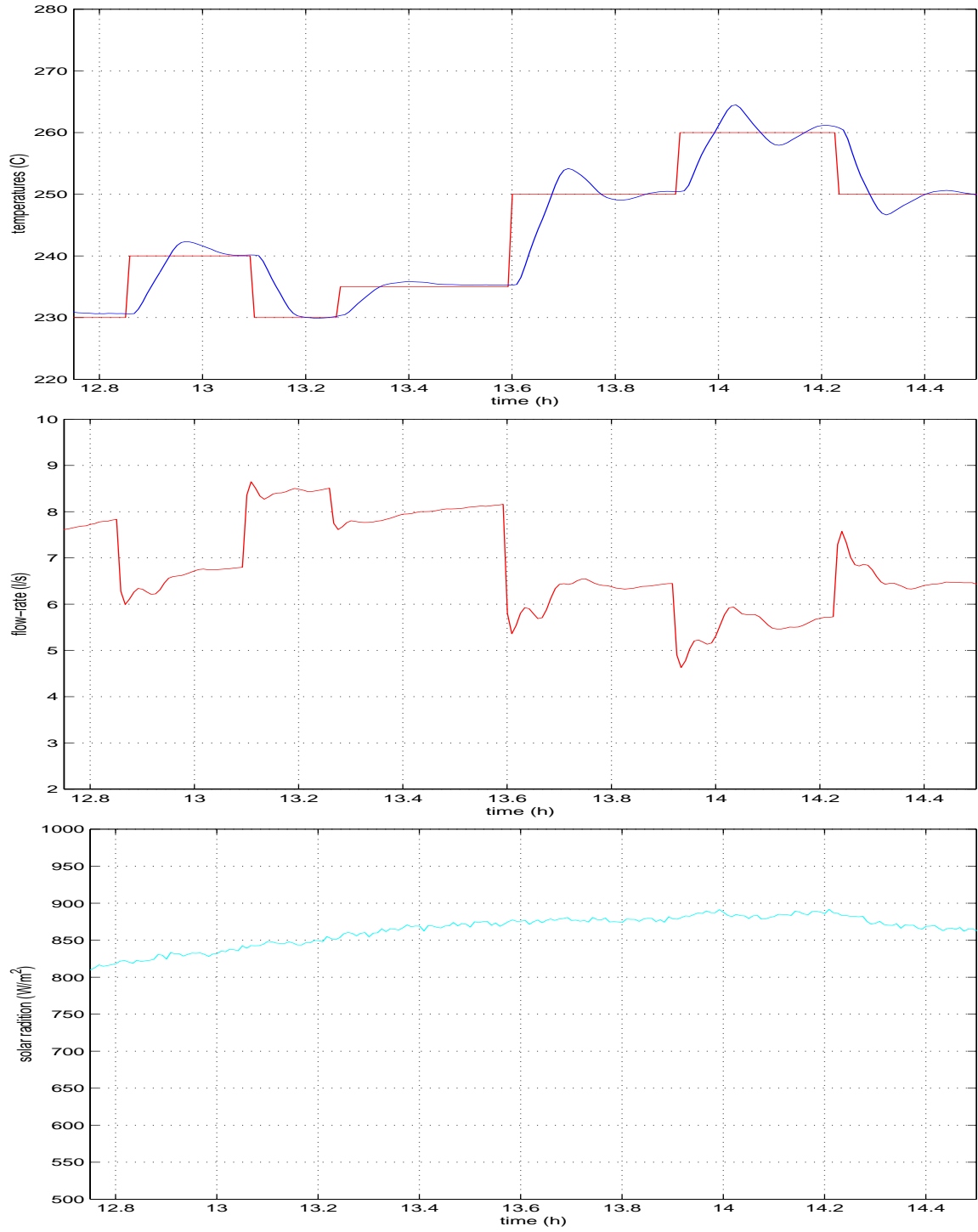


Figure 15: Experimental results with a linear controller designed for the 8 l/s operating point, 14 July 1998.

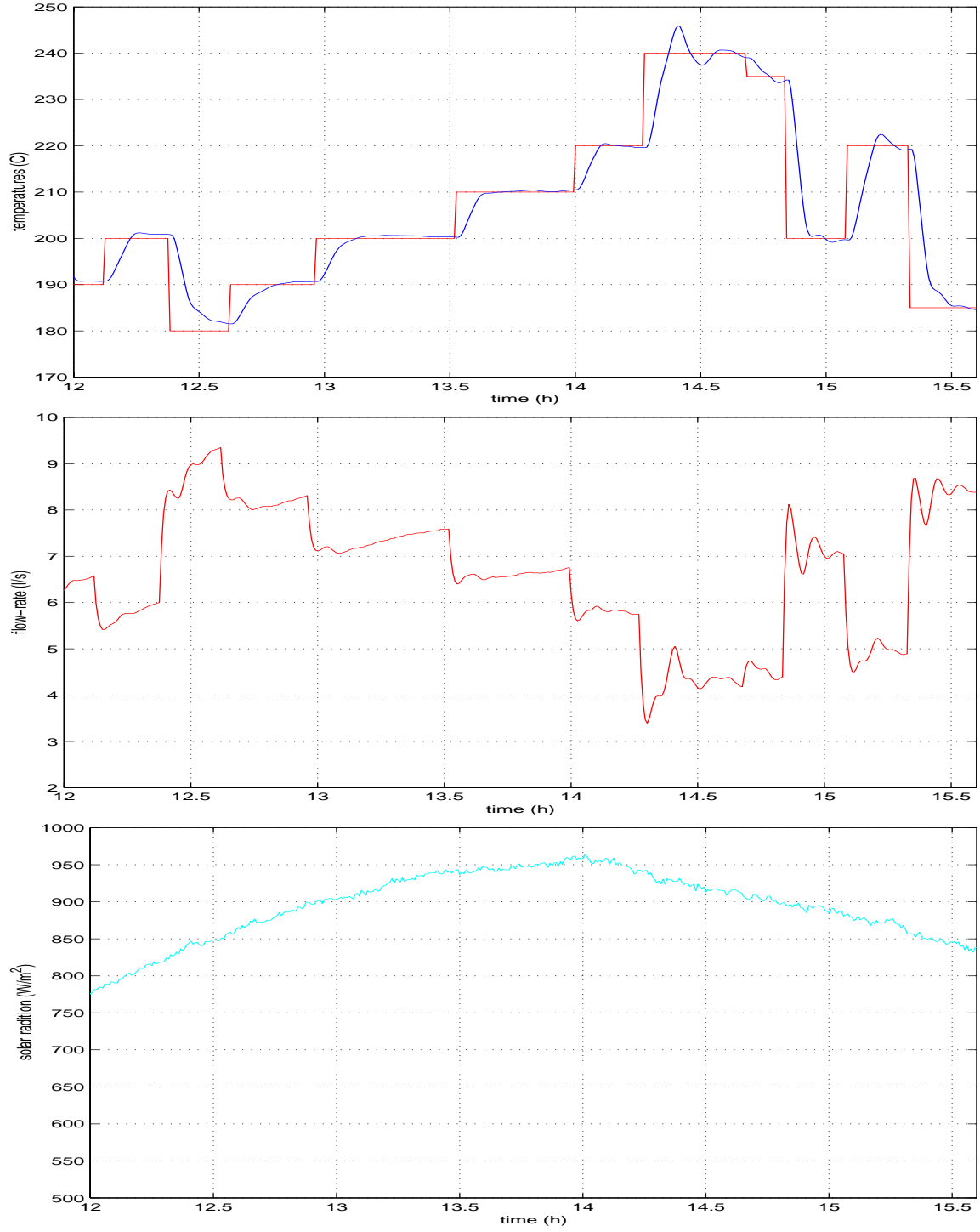


Figure 16: Experimental results with a gain-scheduled controller, 8 September 1998.

reason for this is that our approach is based on more accurate higher-order local models while the lower order models used in (Pickhardt 1998, Rato *et al.* 1997) cannot be expected to capture the anti-resonant modes. Another reason is that the local controllers are scheduled on the actual oil flow rate in our approach rather than the predicted steady-state oil flow rate, as in (Pickhardt 1998), or local model performance measures, as in (Rato *et al.* 1997), both of which correspond to lower bandwidth in the scheduler.

There are two major sources of disturbances. First, the solar radition is subject to fairly deterministic 24 h periodic variations. Second, the solar radition is subject to random clouds and other atmospheric disturbances. A period of 24 h corresponds to a frequency of $\omega = 7.3 \cdot 10^{-5}$ rad/s. At this frequency we observe from the Bode plot in Figure 14 that output disturbances are damped by approximately -36 to -44 dB, depending on the operating point. Note that a reduction of the bandwidth in the 4 l/s regime, as suggested above, would lead to less damping of the output disturbances in this regime, but a more uniform disturbance rejection performance over the operating range. Typically, the periodic variations of the solar radition corresponds to an output temperature variation around $\pm 40^\circ\text{C}$ (from 0 to 80). Thus, the controller will reduce the output temperature variations to about $\pm 0.2^\circ\text{C}$ to $\pm 0.8^\circ\text{C}$, depending on the operating point. In order to study the rejection of random disturbances due to clouds, a simulation experiment was carried out (since no natural disturbances occurred during the experiments). The controller was simulated with the experimental solar radition time-series in Figure 16 but with 3 artificial "clouds" superimposed. An experimentally verified distributed parameter model of the plant, similar to (Camacho *et al.* 1997), was used in the simulator. Thus, the simulation results shown in Figure 17 are subjected to unmodelled dynamics. In particular, the simulation model does not fully describe the heat losses to the environment, which leads to a steady-state difference in the oil flow rate between the simulator and experiments. However, this is not important in these simulations since the controller has integral action. Moreover, the simulation results contain a larger amount of high-frequency components. The reason for this is that the high-frequency phenomena, such as mixing, heat conduction and heat capacity of the tube, are neglected from the simulation model since they are well above the bandwidth of the controller. In order to compare the simulation model with the true plant, during the first part of the simulation the setpoint, inlet temperature and disturbance are identical to the experimental time-series in Figure 16. The results shows that the simulations are fairly realistic, and that the disturbance rejection is satisfactory. However, it is evident that disturbance rejection could be further improved by adding a feedforward from the corrected solar radiation.

It is well known that slow variation of the scheduling variables is a sufficient condition for stability of gain scheduled control (Shamma and Athans 1990, Hunt and Johansen 1997). Since the input is used for scheduling, this condition is clearly not met in this case since the input varies at approximately

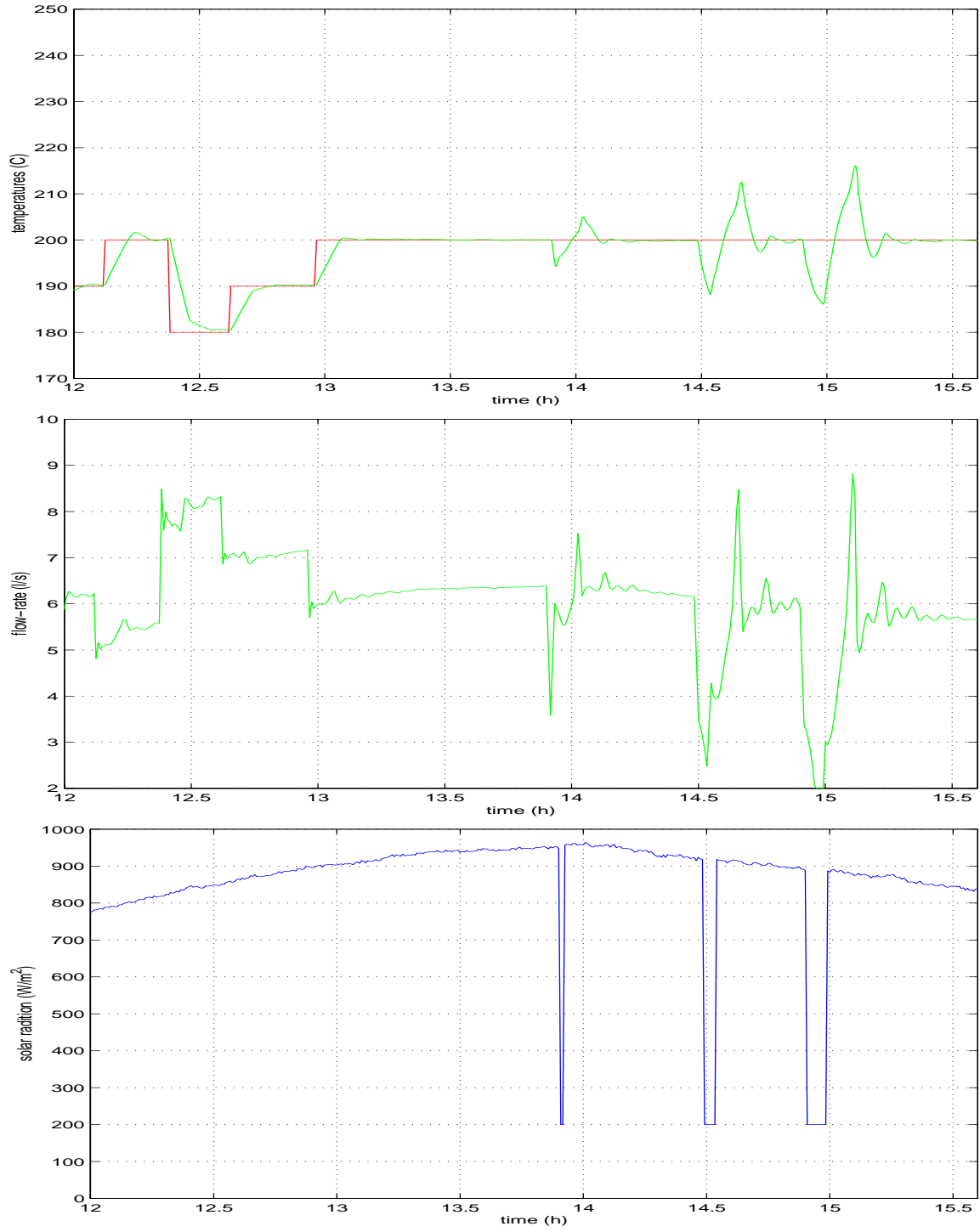


Figure 17: Simulation results with a gain-scheduled controller, where the solar radiation has artificially imposed clouds.

the same rate as the output. However, it is also clear that this is not a necessary condition in many cases (as "proven" by the experiments in this case). It can be seen from the experimental results that the local controllers and their interpolation functions are tuned using careful engineering design such that no significant transients or oscillations appear when moving between operating regimes. The claimed stability is further supported by a range of other experiments and simulations with the same or similar controllers but different setpoint and setpoint changes. Figure 18 illustrates the open loop transfer function for all 9 combinations of the 3 local linear models in regimes R1, R2 and R3 and the 3 local linear controllers in regimes R1, R2 and R3. It can be seen that in all 9 cases the closed loop is stable with some gain and phase margins. Although not a proof of stability, this suggests that the control design is robustly stabilizing.

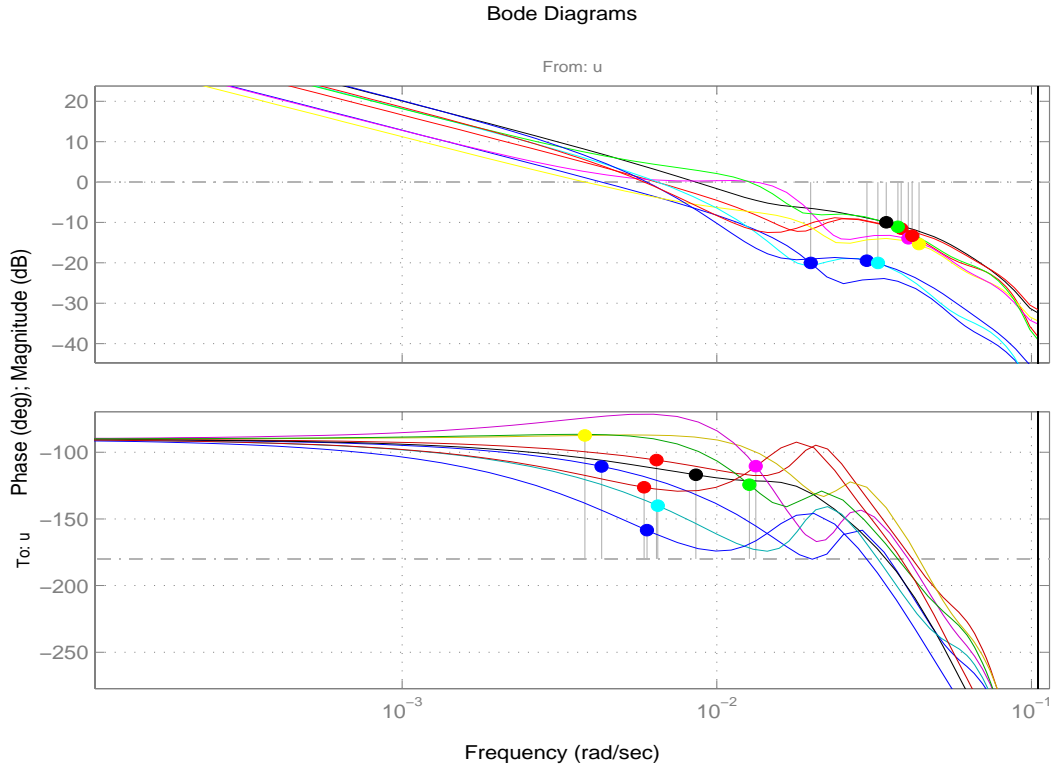


Figure 18: Bode plots of the open loop transfer functions from all combinations of the local models in regimes R1, R2 and R3 with the local linear controllers for regimes R1, R2 and R3.

7 Conclusions

A gain-scheduled pole placement control strategy designed on the basis of local linear ARX models was experimentally tested on a pilot-scale solar power plant. The results show that the gain-scheduled control strategy performs very well when compared to other experimental studies on the same plant available in the open literature. The results with a linear controller shows that good

performance can only be achieved in a small operating regime with a linear controller. Hence, the need for a nonlinear controller is evident. Furthermore, we believe the gain-scheduled pole placement controller's performance could be improved by fine tuning the local models and controllers. However, this was not possible due to limited access to the plant.

Acknowledgements

The work was, in part, sponsored by the European Commission under the TMR programme. The authors are grateful for the support given by the staff at Plataforma Solar de Almeria.

References

- Åström, K. J. and B. Wittenmark (1997). *Computer Controlled Systems: theory and design*. Prentice-Hall. Third Edition.
- Camacho, E. F., M. Berenguel and F. R. Rubio (1994). Application of a gain scheduling generalized predictive controller to a solar power plant. *Control Engineering Practice* **2**, 227–238.
- Camacho, E. F., M. Berenguel and F. R. Rubio (1997). *Advanced Control of Solar Plants*. Springer-Verlag, London.
- Hunt, K. J. and T. A. Johansen (1997). Design and analysis of gain-scheduled local controller networks. *Int. J. Control* **66**, 619–651.
- Johansen, T. A., K. J. Hunt and H. Fritz (1998). A software environment for gain scheduled local controller network design. *IEEE Control Systems Magazine* **18**(2), 48–60.
- Meaburn, A. and F. M. Hughes (1993). Resonance characteristics of distributed solar collector fields. *Solar Energy* **51**, 215–221.
- Pickhardt, R. (1998). Application of adaptive controllers to a solar power plant using a multi-model description. In: *Proceedings of the American Control Conference, Albuquerque, NM*.
- Rato, L., D. Borrelli, E. Mosca, J. M. Lemos and P. Balsa (1997). MUSMAR based switching control of a solar collector field. In: *Proceedings of the European Control Conference, Brussels*.
- Rugh, W. J. (1991). Analytical framework for gain scheduling. *IEEE Control Systems Magazine* **11**(1), 79–84.
- Shamma, J. S. and M. Athans (1990). Analysis of gain scheduled control for nonlinear plants. *IEEE Trans. Automatic Control* **35**, 898–907.

Silva, R. N., L. M. Rato, J. M. Lemos and F. Coito (1997). Cascade control of a distributed collector solar field. *J. Process Control* **7**, 111–117.